Role of smooth muscle activation in the static and dynamic mechanical characterization of human aortas

Giulio Franchini[a], Ivan D. Breslavsky[a], Francesco Giovanniello[a], Ali Kassab[a,b], Gerhard A. Holzapfel[c,d], and Marco Amabili[a,e,1]

[a]Department of Mechanical Engineering, McGill University, Montreal, QC H3A 0C3, Canada; [b]Research Center, Centre Hospitalier Universitaire de Montréal, Université de Montréal, Montreal, QC H2X 3E4, Canada; [c]Institute of Biomechanics, Graz University of Technology 8010 Graz, Austria; [d]Department of Structural Engineering, Norwegian University of Science and Technology 7034 Trondheim, Norway; and [e]Advanced Material Research Center, Technology Innovation Institute, Abu Dhabi, UAE

Edited by Yonggang Huang, Northwestern University, Glencoe, IL; received September 22, 2021; accepted December 2, 2021

Experimental data and a suitable material model for human aortas with smooth muscle activation are not available in the literature despite the need for developing advanced grafts; the present study closes this gap. Mechanical characterization of human descending thoracic aortas was performed with and without vascular smooth muscle (VSM) activation. Specimens were taken from 13 heart-beating donors. The aortic segments were cooled in Belzer UW solution during transport and tested within a few hours after explantation. VSM activation was achieved through the use of potassium depolarization and noradrenaline as vasoactive agents. In addition to isometric activation experiments, the quasistatic passive and active stress–strain curves were obtained for circumferential and longitudinal strips of the aortic material. This characterization made it possible to create an original mechanical model of the active aortic material that accurately fits the experimental data. The dynamic mechanical characterization was executed using cyclic strain at different frequencies of physiological interest. An initial prestretch, which corresponded to the physiological conditions, was applied before cyclic loading. Dynamic tests made it possible to identify the differences in the viscoelastic behavior of the passive and active tissue. This work illustrates the importance of VSM activation for the static and dynamic mechanical response of human aortas. Most importantly, this study provides material data and a material model for the development of a future generation of active aortic grafts that mimic natural behavior and help regulate blood pressure.

mechanical characterization | microstructural characterization | vascular smooth muscle activation | mechanical material model | human aorta

The rupture of aortic aneurysms causes around 10,000 deaths each year in the United States (1). Surgical repair of aortic aneurysms and aortic dissections absorb significant healthcare resources (2). Prosthetic tubes made of polyester (Dacron) or polytetrafluoroethylene are often used for the surgical repair of large arteries in aneurysms or acute dissection. Unfortunately, these grafts are so stiff to diameter expansion (3) that they can cause cardiovascular and perfusion problems because they fail to reduce the highly pulsatile nature of the blood flow exiting the heart. This is the reason for an increasing interest in the development of a new generation of grafts (4) in innovative biomaterials or in tissue engineering that mimic the dynamic behavior of the aorta, which is achieved through the correct adjustment of mechanical properties and the introduction of a layered design. Arteries respond to vasoactive chemical stimuli by varying their mechanical properties and diameter because of vascular smooth muscle (VSM) activation; this helps in regulating blood pressure (5). We envision a future generation of aortic grafts based on tissue engineering that mechanically respond to vasoconstrictors to maintain this function. To achieve this result, it is first necessary to investigate the relationship between VSM activation and the mechanical properties of the aorta and to develop a suitable model of the active mechanical response for the graft design. Since the VSM is mainly located in the tunica media (some cells can infiltrate the intima and adventitia with increasing age), the activation strain can be attributed to this aortic layer. Experimental data and a suitable material model for human aortas with smooth muscle activation are not available in the literature despite the need for the development of advanced grafts. This appears to be due to the difficulty of obtaining suitable human samples. In fact, VSM activation is only possible for a small number of hours after the explantation from a heart-beating donor (i.e., donor in intensive care unit with neurological determination of death) and when the tissue is kept refrigerated in organ preservation solution all the time before testing. The present study is important as it provides much-needed experimental data. These data made it possible to create a precise structure-based model of the active aortic tissue and to identify the corresponding material parameters.

The passive (i.e., without VSM activation) quasistatic mechanical properties of the intact wall of the human aorta and its three individual layers have been extensively investigated experimentally. In particular, uniaxial extension tests were carried out on

Significance

The rupture of aortic aneurysms causes around 10,000 deaths each year in the United States. Prosthetic tubes for aortic repair present a large mismatch of mechanical properties with the natural aorta, which has negative consequences for perfusion. This motivates research into the mechanical characterization of human aortas to develop a new generation of mechanically compatible aortic grafts. Experimental data and a suitable material model for human aortas with vascular smooth muscle (VSM) activation are not available. Hence, the present study provides experimental data that are needed. These data made it possible to develop a precise structure-based model of active aortic tissue. The results show the importance of VSM activation on the static and dynamic mechanical response of human aortas.

Author contributions: M.A. designed research; G.F., I.D.B., F.G., A.K., and M.A. performed research; G.F., I.D.B., F.G., and M.A. analyzed data; and G.F., I.D.B., G.H., and M.A. wrote the paper.

The authors declare no competing interest.

This article is a PNAS Direct Submission.

[1]To whom correspondence may be addressed. Email: marco.amabili@mcgill.ca.

This article contains supporting information online at http://www.pnas.org/lookup/suppl/doi:10.1073/pnas.2117232119/-/DCSupplemental.

Published January 12, 2022.

strips (cut in the circumferential and longitudinal directions) from the intact wall or separated layers (6–9), and biaxial tests on squares and cruciform samples of aortic tissue (10, 11) were conducted. The microstructure of the collagen and elastin fiber distributions in the three layers was also examined in detail using second-harmonic generation and two-photon excited fluorescence microscopy (9, 10, 12). Along with the progress of experiments, advanced structure-based material models have also been refined. It was assumed that a ground substance/elastin matrix is reinforced by collagen fibers. The orientations and dispersions of the collagen fiber identified from experiments were taken into account in the more advanced models (13–15). The passive dynamic material properties (also referred to as viscoelastic) of the human aortas, on the other hand, are much less studied, even if they are of great importance since the aorta is dynamically loaded by pulsating pressure under physiological conditions. The experiments were performed on a mock circulatory loop under physiological pulsatile pressure and flow (3, 16) and on strips of thoracic descending aortas (8, 17). Viscoelastic models have been developed (18, 19), but they can only partially describe the experimental results. Experimental data show that the aorta stiffens with increasing age (8, 9, 11), which favors hypertension (20).

The active (i.e., with VSM activation), quasistatic mechanical characterization of arteries has been less studied than its passive counterpart. The number of studies on human samples is very limited (21, 22), and none have been found on large arteries. Vasoactive agents commonly used to induce VSM contraction are potassium depolarization (KCl) (23), noradrenaline (22), norepinephrine (21), and phenylephrine (24). By using different concentrations of agents, different degrees of activation can be achieved. In previous studies, two methodologies of activation experiments were carried out: 1) pressurization of arterial segments (21, 24–29) and 2) extension tests on arterial strips and rings (5, 22, 30–32). Experiments on strips and rings can be isometric, in which the sample is constantly stretched, and the increase in force from the passive to the active state is measured (5); these are the typical experiments that are carried out on a myograph (22). In isobaric experiments performed on arterial segments, the pressure and axial stretch are fixed; activation of the VSM leads to a reduction in diameter (5). Approximation formulas allow the change in diameter to be linked to the arterial stiffness. Another type of experiment can be performed to measure the force-displacement curve (then converted to stress/strain) in the case of VSM activation by following a similar procedure used for passive mechanical characterization (6–9). A comparison of the active and passive curves gives the mechanical characteristics of the VSM activation. Excluding refs. 5, 28, and 30, a literature review shows that activation was only measured in the circumferential direction. Indeed, the orientation of VSM cells in arteries has usually been believed to be almost circumferential; the present study shows that this is not the case with the descending thoracic aorta in humans. Mechanical models of the mechanical response of active arteries have been developed (5, 14, 33–39) but generally only consider activation in the circumferential direction. There are two exceptions: the model in ref. 5 introduces independent activation stresses in the circumferential and axial directions; another study (38) considers two helically arranged symmetric families of VSM without fiber dispersion.

In the present study, the active and passive mechanical characterization of human descending thoracic aortas was performed on specimens from 13 heart-beating donors. The aortic segments were cooled in Belzer UW solution during transport and tested within a few hours after explantation. VSM activation was achieved through the use of KCl and noradrenaline as vasoactive agents. In addition to isometric activation experiments, the quasistatic passive and active stress–strain curves for circumferential and longitudinal strips of the aortic material were obtained. This characterization made it possible to build an original mechanical model of the active aortic material that exactly matched the experimental data. The dynamic mechanical characterization was also performed using cyclic strain at different frequencies of physiological interest. An initial prestretch, which corresponded to the physiological conditions, was applied before the cyclic loading. Dynamic tests allowed to identify the differences in the viscoelastic behavior of the passive and active tissue. The influence of age was also studied. The present study illustrates the importance of VSM activation for the static and dynamic mechanical response of human aortas. Most importantly, it provides material data for the development of a future generation of active aortic grafts that mimic the natural behavior.

Results and Discussion

The results are presented for 13 descending thoracic aortas from heart-beating donors with 25 to 68 y of age (mean age = 48.6 ± 14.2 y). Information on donors can be found in *SI Appendix*, Table S1. Fig. 1 illustrates the experimental procedure of the mechanical tests. Circumferential and longitudinal strips—about 5 mm wide and 35 mm long—were immersed in Krebs–Henseleit buffer solution, bubbled with oxygen, and kept at a temperature of 37 °C. The time diagram in Fig. 1*F* shows the various phases of each test on a strip that takes just over 2 1/2 h. First, a passive quasistatic mechanical characterization is carried out, which includes preconditioning, followed by a dynamic characterization with two fixed levels of prestress. Isometric VSM activation is then induced at about 50 kPa engineering prestress by first using potassium depolarization (KCl, 60 mM) followed by the addition of noradrenaline (18 μM). The combined use of two vasoactive agents and their concentration enables a VSM contraction that comes very close to the maximum possible for the specimen (22). Under physiological conditions, the VSM activation is between zero and the maximum, depending on the concentration of the vasoactive agents in the blood.

A quasistatic mechanical characterization with preconditioning followed by a dynamic characterization at the same two prestress levels is carried out on the tissue with VSM activation. The measured stresses versus time corresponding to the isometric activation are presented in Fig. 2*A* for the strips of donor VIII in both directions. The time of insertion of each vasoactive agent is indicated by an arrow. The results for all samples are shown in *SI Appendix*, *Isometric experiments on activation*. A statistical analysis of the activation stresses for all circumferential and all longitudinal strips together and divided into two age groups (25 to 48 y; 55 to 68 y) is presented in Fig. 2 *B* and *C*. While the results show larger activation stresses for the circumferential strips (median of all donors = 22.2 kPa), the activation stress in the longitudinal direction is also significant (median of all donors = 14.9 kPa), which is only 33% smaller than that in the circumferential direction. The activation stress seems to decrease with age. The median for the circumferential strips decreases from 25.7 (25 to 48 y) to 21.6 kPa (55 to 68 y); for the longitudinal strips, the median is reduced from 16.8 (25 to 48 y) to 7.8 kPa (55 to 68 y). An ANOVA test indicates a clear statistical difference between the two age groups for the activation stress of the longitudinal strips (P value = 0.0391), while for the circumferential strips, likely there is no difference (P value = 0.7274).

Microstructural Characterization. In order to elucidate the mechanism of activation both in the circumferential and in the longitudinal direction, the distribution of the VSM cell orientations in the tunica media of donors IV and VIII is examined in Fig. 3.

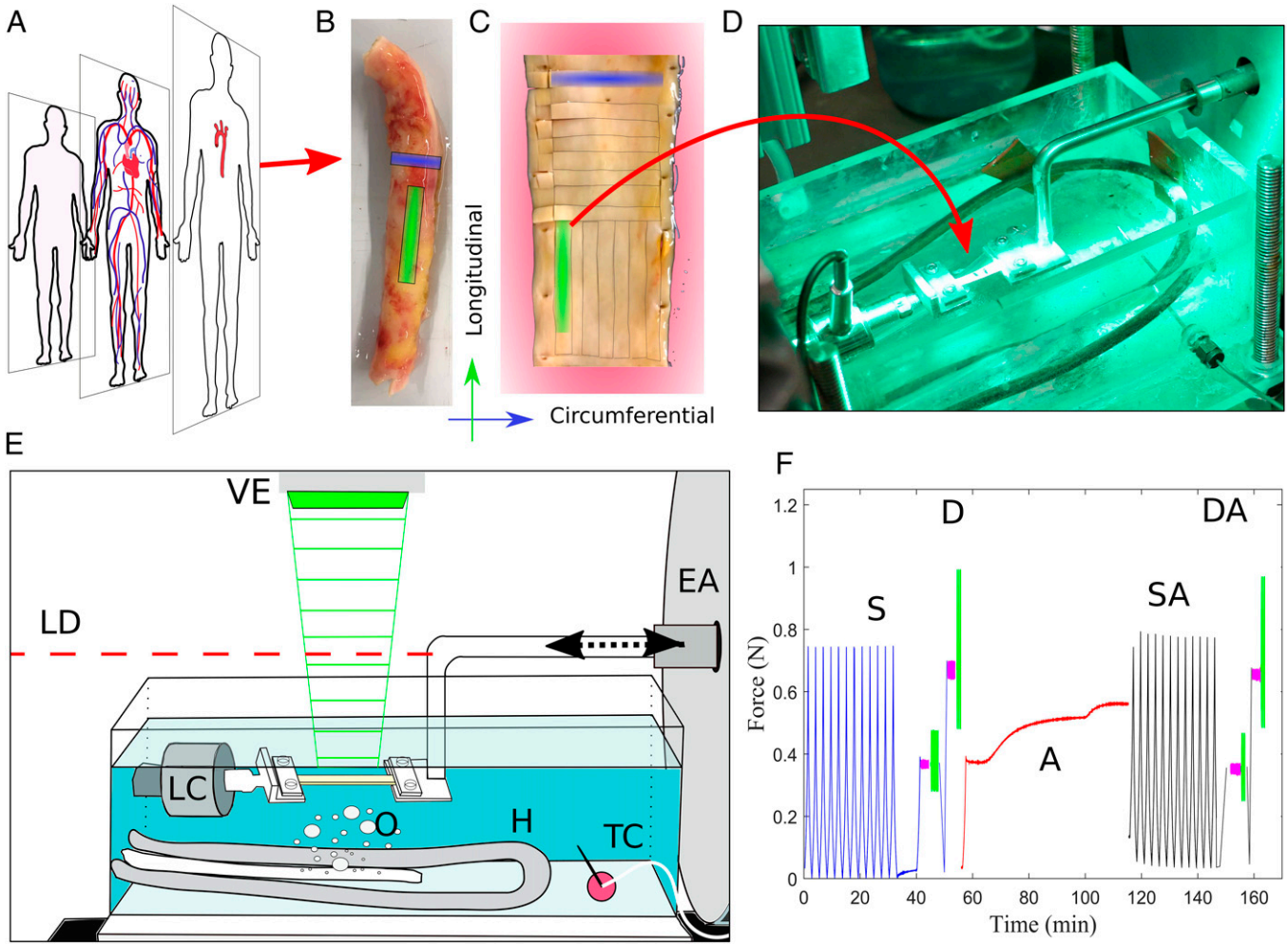

Fig. 1. Specimen preparation and experimental setup. (*A*) Position of the thoracic aorta in the human body. (*B*) Descending thoracic aorta from donor IV with indication of circumferential (blue) and longitudinal (green) strips. (*C*) Aorta from donor IV opened with a longitudinal cut on the posterior side. Circumferential and longitudinal strips are cut with a punch. (*D*) Photo of the experimental setup for quasistatic and dynamic uniaxial tensile tests with the thermal control, the strip holders, and the aortic strip installed. (*E*) Scheme of the experimental setup. VE, video extensometer; LD, laser Doppler sensor; EA, electrodynamic actuator; LC, load cell; O, tube carrying oxygen (O2) for bubbling the solution; H, heater; TC, temperature control. (*F*) Typical phases of an experiment on a strip described by the measured force (N) versus time (in minutes). S, quasistatic mechanical characterization of the passive strip reaped several times to achieve preconditioning; D, dynamic tests on the passive strip with harmonic loading at two levels of preload performed at frequencies from 1 to 5 Hz; A, isometric activation of the strip, first with KCl followed by noradrenaline; SA, quasistatic mechanical characterization of the active strip; DA, dynamic tests on the active strip with harmonic loading at two levels of preload carried out at frequencies from 1 to 5 Hz.

Traditional histology with a Masson trichrome stain is shown first in Fig. 3*A* for a cross-section (i.e., through the thickness) and in Fig. 3*B* for an in-plane section (i.e., parallel to the strip surface). While the VSM cells (red in Masson-stained section) appear well organized with parallel fibers in the cross-section, the directional distribution in an in-plane section is quite dispersed. In order to quantify the dispersion of the VSM cell orientation, in-plane sections were stained with DRAQ5 (1/1,000, 30 min) in order to make the nuclei in VSM cells visible. The tissue was excited by a laser at 638 nm, and light was captured above 650 nm with a Leica confocal microscope. The nuclei appear violet in the image in Fig. 3*C*, and since they are elongated, their direction distribution is evaluated by an image-processing code (9), which gives the histogram of the in-plane dispersion. The histogram in Fig. 3*D* shows that the VSM is dispersed, with a peak in the orientation distribution in the circumferential direction and a practically symmetric distribution around the peak. This excludes shear strains through activation in uniaxial tensile tests. Additional results on the microstructural characterization are presented in *SI Appendix*, *Additional results for microstructural characterization*, which shows a larger dispersion of the VSM distribution for a different aorta. The microstructural analysis justifies the observed activation in both directions with a larger force in the circumferential direction.

Quasistatic Mechanical Characterization. Uniaxial extension tests were carried out after preconditioning at a low strain rate to characterize the active and passive static behavior of aortic strips. Fig. 4*A* shows the passive and active engineering stress–strain behavior for the circumferential and longitudinal strips of donor VIII. While the passive curves start from the origin, both active ones have an initial positive stress at the original zero strain because of the VSM contraction. The difference between the active and passive curves in Fig. 4*A* at prestretch corresponding to 50 kPa is a bit larger (23% in circumferential direction and 21% in longitudinal direction) than the total activation stress given in Fig. 2*A* due to the preconditioning and the fact that this is not an isometric test, but the strip is continuously elongated. This phenomenon is observed also for the other tested aortas, with very few exceptions. Other features in Fig. 4*A* are that the

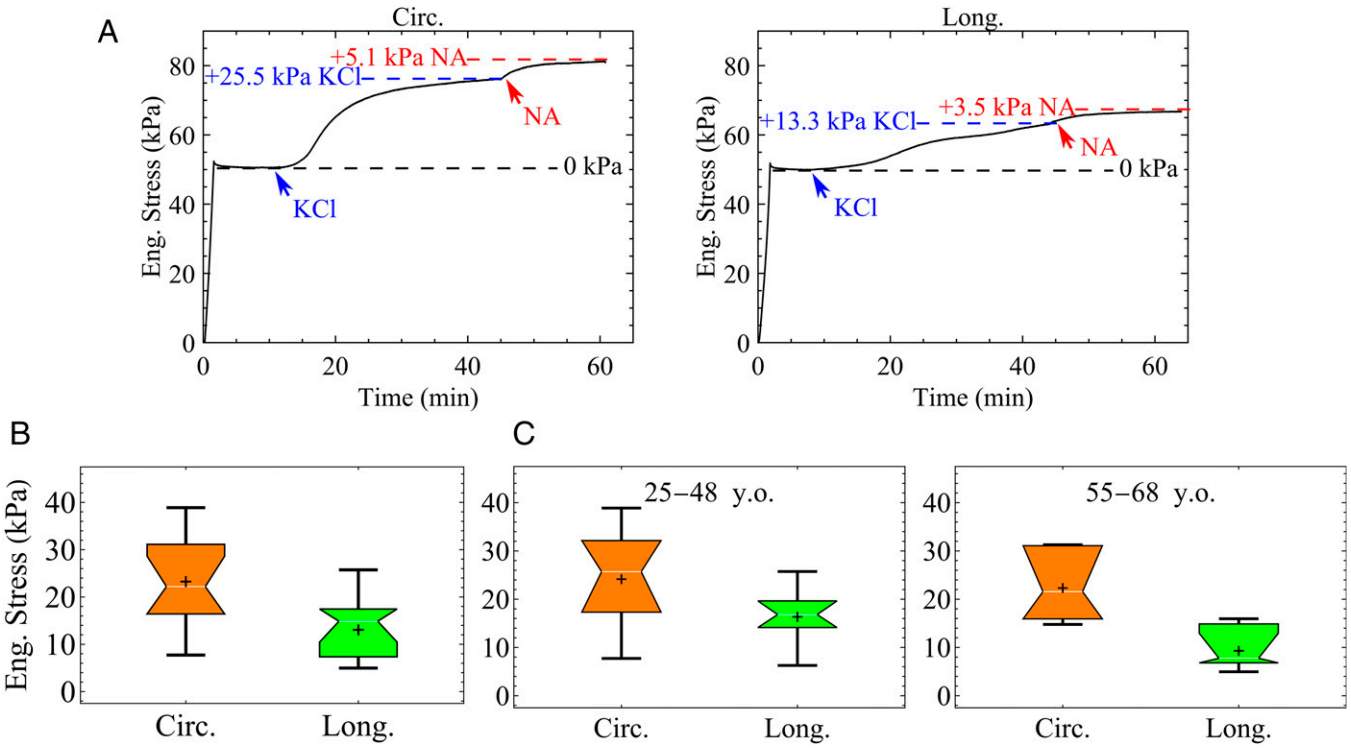

Fig. 2. Isometric activation of aortic strips. (*A*) Activation of the circumferential and longitudinal strips from donor VIII as stress developed over time. The time of injection of the vasoactive agent—first KCl, followed by noradrenaline (NA)—is indicated as well as the corresponding increase in stress. (*B*) Statistical analysis of the activation stress for the circumferential and longitudinal strips from 13 donors at a prestretch corresponding to 50 kPa (engineering stress); maximum, minimum, first quartile, third quartile, median (white horizonal line in the box), and average (+) are reported. (*C*) Statistical analysis of the activation stress divided into two age groups: 22 to 48 y (seven donors) and 55 to 68 y (six donors).

active curves are above the passive ones (i.e., higher stresses are obtained at the same strain) and are significantly less curved (more linear). These stress–strain curves allow material parameters to be identified for the active and passive material once a material model has been built. Material parameters of healthy aortic tissues are necessary to design grafts that mimic the mechanical behavior of the native aorta. The stress–strain curves for all strips tested are given in *SI Appendix*, *Active and passive quasi-static extension tests*.

Mechanical Model of the Activated Tissue. The strain–energy function W of the aortic wall is represented as the sum of the passive and active components

$$W = W^P + W^A, \qquad [1]$$

where the passive component W^P is given in ref. 9 and described in *SI Appendix*, *Details on the material model of the passive and active aortic tissue*. It is a microstructurally based model that presents 1) an isotropic term to describe the elastin network and the ground substance, 2) one family of collagen fibers taking into account their orientation dispersion, and 3) an orthogonal fiber family to describe the cross-link and lateral interaction of the collagen fibers. The active term refers to the activation of the VSM. It is assumed that the fibers of VSM are not perfectly aligned in the circumferential direction but rather dispersed around the circumferential direction of the aorta in the plane tangent to the middle surface (in plane) of the strip. In addition to the main family of dispersed VSM, a second orthogonal family with the same dispersion is considered to describe the lateral interaction between VSM fibers; this is due to the interwoven VSM fibers shown in Fig. 3*B*. This second family is assumed to contribute with a minor active stress than the main family. The proposed active strain–energy function is given by

$$W^A = \tilde{K}\sum_{i=1}^{2} K_i\left[E_i^{VSM} + \frac{a_i}{2}\left(E_i^{VSM}\right)^2 - \frac{b_i}{m_i+1}\left(E_i^{VSM}\right)^{m_i+1}\right], \qquad [2]$$

where $a_i, b_i > 0$ and m_i are integers larger than one and

$$E_1^{VSM} = 2\left[\kappa_{IP}^{VSM}\left(\varepsilon_{xx}+\varepsilon_{\theta\theta}\right) + \left(1-2\kappa_{IP}^{VSM}\right)\varepsilon_{\theta\theta}\right], \qquad [3a]$$

$$E_2^{VSM} = 2\left[\kappa_{IP}^{VSM}\left(\varepsilon_{xx}+\varepsilon_{\theta\theta}\right) + \left(1-2\kappa_{IP}^{VSM}\right)\varepsilon_{xx}\right], \qquad [3b]$$

while ε_{xx} and $\varepsilon_{\theta\theta}$ are the longitudinal and circumferential normal Green–Lagrange strains, and $\tilde{K}$ is the activation-level coefficient having a value comprised between 0 (no activation) and 1 (maximum activation). Eqs. **3a** and **3b** are inspired by an expression for the bidimensional fiber dispersions proposed in ref. 15. Expression (Eq. **2**) has nine parameters, K_i, a_i, b_i, m_i, κ_{IP}^{VSM}. The first term within the brackets in Eq. **2** takes into account the stress value at zero principal strain. In particular, K_i is a stress-like parameter associated with the initial active stress values. Since the initial stress at zero strain is generally different in the axial and circumferential directions, the model captures this feature through the VSM dispersion parameter κ_{IP}^{VSM}. The second term within the brackets in Eq. **2** reflects the relatively slow initial growth of the activation stress with strain, which is controlled by the parameter a_i. The third term represents the rapid decrease in the activation stress after a certain strain value because of a higher power; the slope of this drop is controlled by the two parameters b_i and m_i. The integer power m_i enables the experimentally observed behavior of the difference between the active and passive mechanical response to be reproduced. The optimization procedure for determining the material parameters is shown in *SI Appendix*, *Details on the material model of the passive and active*

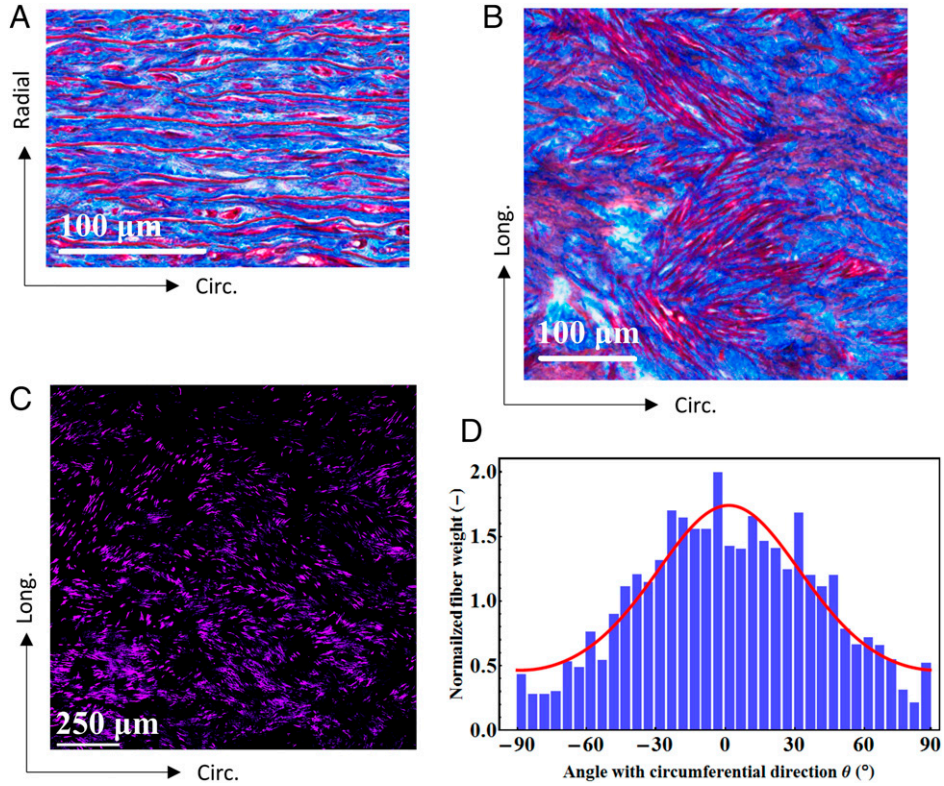

Fig. 3. Microstructural analysis of tunica media. (*A*) Cross-section (5 μm thick) with Masson trichrome stain (VSM in red) from donor IV. (*B*) In-plane section (5 μm thick) with Masson trichrome stain (VSM in red) from donor IV. (*C*) In-plane section with DRAQ5 stain (nuclei of VSM in violet) from donor VIII. (*D*) Histogram showing the distribution of the VSM directions from image *C* with the red line of the fitted distribution; dispersion coefficient $\kappa_{IP}^{VSM} = 0.343$.

aortic tissue. The dispersion parameter κ_{IP}^{VSM} is obtained by fitting a von Mises probability distribution (9, 15), that is,

$$\rho_{IP}(\theta) = \frac{\exp\left[c\cos\left(2\theta\right)\right]}{I_0(c)}, \qquad [4]$$

to the experimental histogram of the VSM distribution in Fig. 3*D* to obtain the concentration parameter c; I_0 is the modified Bessel function of the first kind of order zero. Once a normalization of the area under the distribution (4) is introduced, the dispersion parameter κ_{IP}^{VSM} is given by refs. 9 and 15:

$$\kappa_{IP}^{VSM} = \frac{1}{2} - \frac{I_1(c)}{2I_0(c)}, \qquad [5]$$

where I_1 is the modified Bessel function of the first kind of order one. κ_{IP}^{VSM} takes on values between 0 for perfectly aligned VSM fibers in the circumferential direction and 0.5 for an isotropic response (i.e., identical response in the circumferential and longitudinal directions) of the VSM.

The second Piola–Kirchhoff stresses in the longitudinal and circumferential directions are obtained by

$$S_{xx} = \frac{\partial \hat{W}}{\partial \varepsilon_{xx}} \quad S_{\theta\theta} = \frac{\partial \hat{W}}{\partial \varepsilon_{\theta\theta}}, \qquad \textbf{[6a] and [6b]}$$

where $\hat{W}$ is the function W given in ref. 1 in which the incompressibility condition was inserted. In fact, the aortic tissue is generally considered incompressible (40). One of the two stresses in Eqs. **6a** and **6b** is zero in uniaxial extension tests. This introduces a relationship that is used to link the strains. It is important to note that because of this link, the active term W^A depends on the passive one W^P. This means that the model takes into account the passive mechanical response of the tissue in order to obtain the activation stress. Fibers that are under compression must be excluded in Eqs. **6a** and **6b** (41).

The parameters of the active and passive material model of all the tested aortas are given in *SI Appendix*, Tables S2 and S3. It is interesting that these material parameters were obtained from experiments with maximum activation of the VSM, that is, with $\tilde{K} = 1$. To obtain lower levels of activation corresponding to lower concentrations of vasoactive agents, reduced values of $\tilde{K}$ should be used while maintaining the same material parameters.

The comparison between the material model and the experimental characterization of the aortic tissue of donor VIII is presented in Fig. 4*B* (note the change in the shape of the curves with respect to Fig. 4*A* because of different stress and strain definitions) in which the VSM dispersion parameter $\kappa_{IP}^{VSM} = 0.343$ was obtained from Fig. 3*D*. The comparison of the experimental results and the model (with the identified material parameters) in Fig. 4*B* is very satisfactory for both passive and active behavior. The convexity of the strain–energy function (1) has been verified numerically for the studied cases. The contour plots of W are presented in Fig. 4*C* for the active case of donor VIII, and they are convex.

Dynamic Mechanical Characterization. Due to the viscoelastic behavior, the mechanical response of the aortic tissue to dynamic loading is different from to quasistatic loading. The aorta is subjected to cyclic pulsatile pressure at a frequency in the range of 1 to about 3 Hz (i.e., 60 to 180 beats per minute). The pulsatile pressure is not harmonic (3), but it can be expanded in a Fourier series with harmonic components. In this study, the strips were loaded by a harmonic cyclic strain with an amplitude of 7% of their length. The loading frequencies used in the tests were set from 1 to 5 Hz in 1 Hz steps. Two dimensionless parameters are introduced to describe the viscoelastic behavior: 1) the dynamic

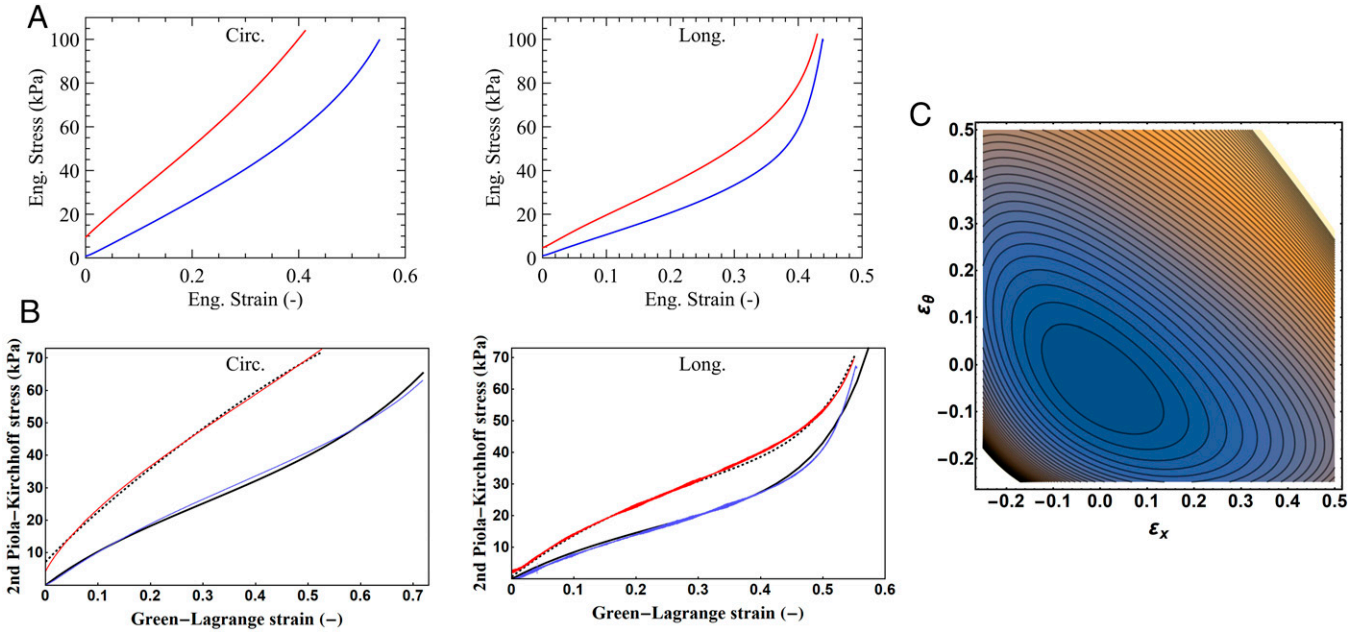

Fig. 4. Quasistatic mechanical characterization and material model. (*A*) Stress–strain curves (engineering stress and engineering strain) from quasistatic uniaxial tensile tests on active (red) and passive (blue) circumferential and longitudinal strips from donor VIII. (*B*) Stress–strain curves (second Piola–Kirchhoff stress and Green–Lagrange strain) from experiments on active (red) and passive (blue) strips from donor VIII and active (black dashed) and passive (black) material model with identified parameters. (*C*) Contour plot of the strain–energy function *W* of the active aortic wall for the case of donor VIII without fiber exclusion; the convex contours represent states of constant energy.

stiffness ratio, which describes the stiffness increase of the tissue under harmonic loading in relation to quasistatic loading, and 2) the loss factor, which is the percentage of energy loss in a cycle with respect to the elastic energy stored in a quarter of the cycle. Mathematical definitions are given in *SI Appendix*, *Dynamic characterization: dynamic stiffness ratio and loss factor*.

Fig. 5*A* shows the hysteresis loops at 1 Hz superimposed on the quasistatic uniaxial extension tests of the active and passive circumferential and longitudinal strips of donor IV. Cycles were performed at two different initial prestress levels, 50 and 90 kPa (engineering stress), for the center of the loop of each strip. The dynamic stiffness ratio and loss factor versus frequency for the active and passive circumferential and longitudinal strips of donor IV for the two prestress levels are given in Fig. 5 *B* and *C*. The results show that both viscoelastic parameters are hardly influenced by the frequency in the studied range. The dynamic stiffness ratio increases significantly for the active strips for both prestress levels, while the loss factor increases for the two active strips for the first prestress level (50 kPa). This level is a good representation of the physiological condition as described in the *SI Appendix*, *Dynamic characterization: additional data*; therefore, this level is chosen to present a statistical analysis for all strips tested (11 of the 13 aortas were also tested dynamically; the results are presented in *SI Appendix*, Tables S4 and S5 and *Dynamic characterization: additional data*).

Fig. 5*D* shows a statistical analysis of the dynamic stiffness ratio and the loss factor at 1 and 3 Hz (combined) for the circumferential and longitudinal strips from 11 donors at 50-kPa prestress. The median of the dynamic stiffness ratio increases from 1.52 (passive) to 2.07 (active) in the circumferential direction (36% increase); it increases from 1.58 (passive) to 2.16 (active) in the longitudinal direction (37% increase). This shows that the increase in both directions is significant and almost identical, which in turn confirms that the activation in the longitudinal direction is very relevant. The median of the loss factor increases from 0.0686 (passive) to 0.0883 (active) in the circumferential direction (29% increase) and from 0.0730 (passive) to 0.0861 (active) in the longitudinal direction (18% increase). ANOVA tests strongly confirm that dynamic stiffness ratio and loss factor are statistically different before and after activation for both directions ($P < 3.9*10\hat{}-5$ in the four tests, rejecting the hypothesis of no difference). Fig. 5*E* presents a statistical analysis of the viscoelastic parameters that divide the donors into two age groups: 25 to 48 and 55 to 68 y. Both age groups show a significant increase in both viscoelastic parameters with active strips. ANOVA tests suggest that likely there are no age-associated differences for the active viscoelastic parameters.

Conclusions

In summary, the results show that VSM activation has a significant quasistatic stiffness increase of the descending thoracic aortic tissue in both the circumferential and longitudinal directions. This effect diminishes with age in longitudinal direction. A microstructural analysis of the VSM cells in the tunica media confirms their dispersion in the plane parallel to the aortic surface, while in a section through the thickness of the aortic wall, they are well organized and parallel to the surface. An accurate material model was developed for the active tissue, and the material parameters were identified from experiments. Harmonic cyclic loading show that the viscoelastic material properties of the aortic tissue increase significantly with the VSM activation. Since activation of the VSM is relevant to the mechanics and physiology of the aorta (5, 42), the experimental data and material model presented in this study could be used to design and develop a mechanically compatible active aortic graft. The regulation of the vascular tone (i.e., the level of VSM contraction) also plays a key role in hypertension and its treatment (43, 44). Therefore, the relationship between VSM activation and arterial mechanical properties is also relevant to address hypertension.

Materials and Methods

Ethics. This research on human samples has been approved by the Ethics Committee of McGill University. *Transplant Québec* receives organs for research purposes from donors who have consented to both transplant and research organ donation following a diagnosis of brain death.

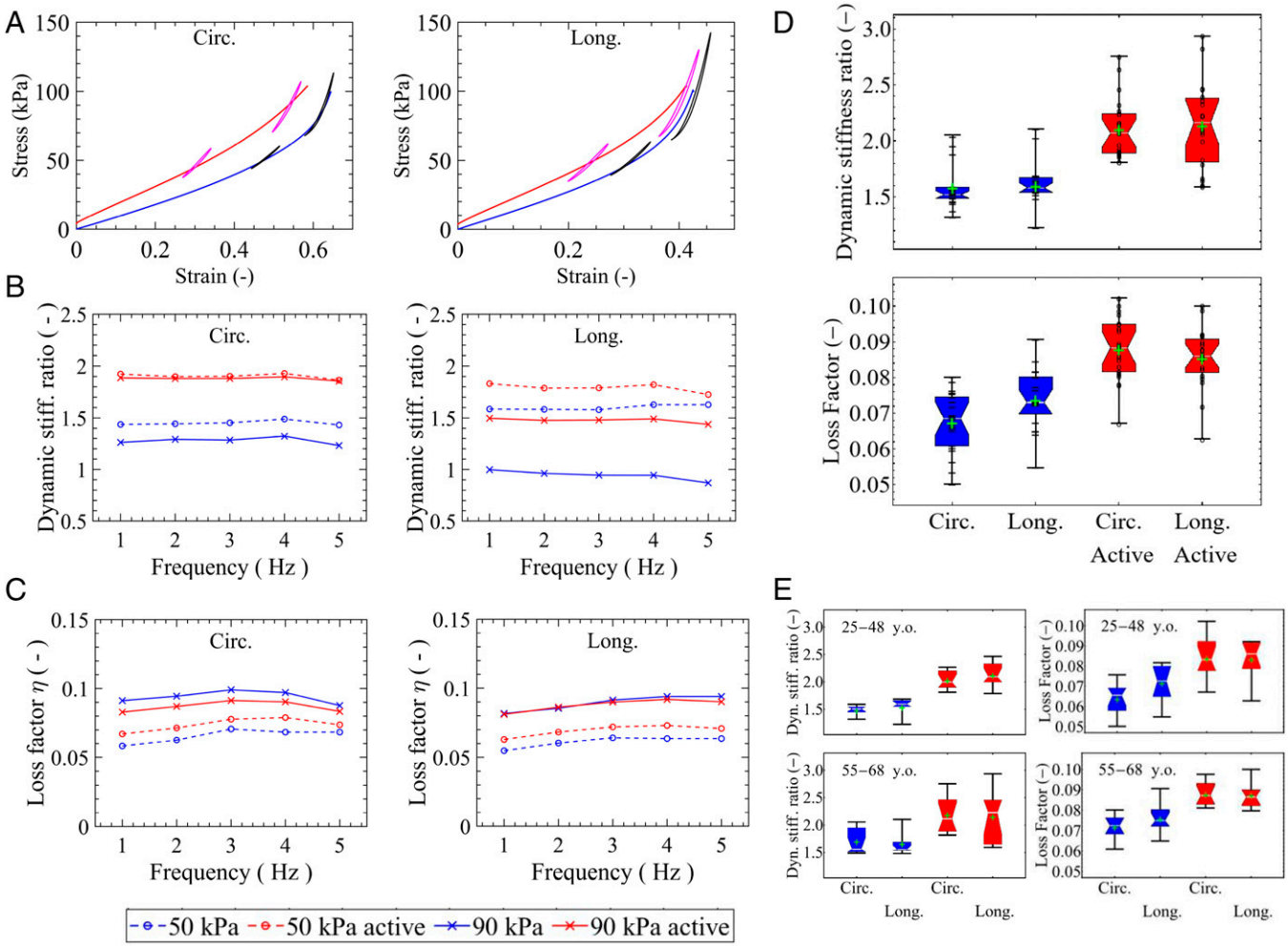

Fig. 5. Dynamic characterization of active and passive aortic strips. (*A*) Hysteresis loops at 1 Hz (active: magenta; passive: black) superimposed to the quasistatic uniaxial tensile tests (active: red; passive: blue) of the circumferential and longitudinal strips from donor IV. Engineering stress versus engineering strain is given. Two cycles at different initial prestretches corresponding to about 50 and 90 kPa for the midpoint of the loop were measured. The amplitude of each cycle was about 0.07 in strain. (*B*) Dynamic stiffness ratio versus frequency for the circumferential and longitudinal strips from donor IV for the two prestress levels (first level 50 kPa; second level 90 kPa). Active: red; passive: blue. (*C*) Loss factor versus frequency. (*D*) Statistical analysis of the dynamic stiffness ratio and loss factor at 1 and 3 Hz for the active (red) and passive (blue) circumferential and longitudinal strips from 11 donors at a prestretch corresponding to 50 kPa (engineering stress); maximum, minimum, first quartile, third quartile, median (white horizonal line in the box), and average (+) are reported. (*E*) Statistical analysis of the dynamic stiffness ratio and loss factor at 1 and 3 Hz for the circumferential and longitudinal strips from the donors, divided into two age groups (25 to 48 and 55 to 68 y) at a prestretch corresponding to 50 kPa; active (red), passive (blue).

Sample Preparation. Descending thoracic aortas from 13 heart-beating donors, aged from 25 to 68 y (mean age = 48.6 ± 14.2 y), were studied. They were collected during a transplant organ donation under a research agreement with *Transplant Québec*, which is the transplant coordinator agency in Québec, Canada. The donors were maintained heart beating after neurological determination of death. All aortas were maintained in Belzer UW organ preservation solution at 4 °C prior to testing. The tissue preparation for experiments consisted of 1) the removal of the periaortic connective tissue and arterial branches, 2) excising the aorta longitudinally at the posterior part between the pair of tiny holes that remain after the intercostal arteries are removed, and 3) obtaining longitudinal and circumferential strips of the approximate dimensions of 5 × 35 mm with a punch of 5 mm wide. The thickness and width of the strips were measured with a Micro-Epsilon triangulation laser sensor (model optoNCDT1402) and caliper at five different locations in order to obtain the cross-sectional area.

Histological analysis was performed on the same strips used in mechanical experiments after discharging the parts in contact with the grips. Samples were processed at the Goodman Cancer Research Centre (GCRC) Histology Core of McGill University. The tissues were dehydrated in 70% ethanol and processed in a Sakura Tissue-Tek vacuum infiltration processor model VIP 6-AI by treating with ethanol, xylene, and paraffin according to a specific protocol. A Leica EG1150 was used for the embedding process. A Leica RM2255 microtome picked up 5-, 10-, and 20-μm-thick sections, which were placed on charged slides (Epic Scientific charged white frosted slides). The slides were placed at 36 °C to remove folds and excess moisture. Paraffin was removed in a Leica ST5020 automatic stainer using a dewaxing protocol. This procedure was performed with the samples already on the slides. Some sections were stained with Masson trichrome using an automatic stainer Leica ST5020. The images were obtained using a Leica Aperio AT Turbo digital pathology scanner. Other sections were stained with DRAQ5 (1/1,000, 30 min) to visualize nuclei in VSM cells.

Mechanical Tests. The experiments were completed within 8 to 10 h of explanting the aorta from the donor's body, which is the time window to obtain proper VSM activation. Since organ explantation are planned only a few hours in advance and are often linked to accidents, the testing team had to be ready for testing any day and at any time not to lose any specimen.

Definitions are as follows: engineering stress is calculated as force divided by undeformed area; engineering strain is calculated as elongation divided by original length.

Quasistatic and dynamic uniaxial extension tests were carried out on a device that was developed for aortic tissue and controlled by a dSPACE hardware with a Simulink code. An Epsilon ONE-52PT video extensometer equipped with a telecentric lens (approximate 5-mm distance between the markers on

the strip; absolute error no greater than ±5 μm) measured the strain in the strip direction, and an Interface model WMCFP 1,000 g load cell obtained the force.

The tested strip was immersed in bubbled (O_2) Krebs–Henseleit buffer solution (D-glucose 2.0 g/L, magnesium sulfate 0.141 g/L, potassium phosphate monobasic 0.16 g/L, potassium chloride 0.35 g/L, sodium chloride 6.9 g/L, calcium chloride 0.373 g/L, and sodium bicarbonate 2.1 g/L) at 37 °C. The distance between the grips had an accuracy of ±1 μm, and the tensile force measurement had an accuracy of ±0.01 N.

The mechanical characterization took place after eight preconditioning cycles with a displacement rate of 0.05 mm/s. It has been verified that this rate is suitable for minimizing viscoelastic effects. Forces were converted into engineering stresses using the cross-sectional area of the strip. The grip distance was adjusted to have an initial load-free position with no sagging of the strip. If necessary, this position was adjusted after preconditioning without a test stop, and the corresponding strain was set to zero.

Data Availability. All study data are included in the article and/or *SI Appendix*.

ACKNOWLEDGMENTS. M.A. acknowledges financial support from the Natural Sciences and Engineering Research Council of Canada (NSERC) Discovery Grant, the NSERC Research Tools and Instruments Grant, and the Canada Research Chair program. Prabakaran Balasubramanian and Giovanni Ferrari assisted with some experiments. Nicolas Audet of the Imaging and Molecular Biology Platform of McGill University helped with the imaging. The GCRC Histology Core of McGill University prepared the samples for histology. We thank *Transplant Québec* for providing the aortas for this research.

1. Centers for Disease Control and Prevention, National Center for Health Statistics, *Underlying cause of death 1999–2018 on CDC WONDER database website*. https://wonder.cdc.gov/ucd-icd10.html. Accessed 20 September 2021.
2. R. S. McClure *et al.*, Economic burden and healthcare resource use for thoracic aortic dissections and thoracic aortic aneurysms – A population-based cost-of-illness analysis. *J. Am. Heart Assoc.* **9**, e014981 (2020).
3. M. Amabili *et al.*, Nonlinear dynamics of human aortas for material characterization. *Phys. Rev. X* **10**, 011015 (2020).
4. T. L. Akentjew *et al.*, Rapid fabrication of reinforced and cell-laden vascular grafts structurally inspired by human coronary arteries. *Nat. Commun.* **10**, 3098 (2019).
5. A. W. Caulk, J. D. Humphrey, S.-I. Murtada, Fundamental roles of axial stretch in isometric and isobaric evaluations of vascular contractility. *J. Biomech. Eng.* **141**, 031008 (2019).
6. H. Weisbecker, D. M. Pierce, P. Regitnig, G. A. Holzapfel, Layer-specific damage experiments and modeling of human thoracic and abdominal aortas with non-atherosclerotic intimal thickening. *J. Mech. Behav. Biomed. Mater.* **12**, 93–106 (2012).
7. S. G. Sassani, J. Kakisis, S. Tsangaris, D. P. Sokolis, Layer-dependent wall properties of abdominal aortic aneurysms: Experimental study and material characterization. *J. Mech. Behav. Biomed. Mater.* **49**, 141–161 (2015).
8. M. Amabili, P. Balasubramanian, I. Bozzo, I. D. Breslavsky, G. Ferrari, Layer-specific hyperelastic and viscoelastic characterization of human descending thoracic aortas. *J. Mech. Behav. Biomed. Mater.* **99**, 27–46 (2019).
9. M. Amabili *et al.*, Microstructural and mechanical characterization of the layers of human descending thoracic aortas. *Acta Biomater.* **134**, 401–421 (2021).
10. J. A. Niestrawska *et al.*, Microstructure and mechanics of healthy and aneurysmatic abdominal aortas: Experimental analysis and modelling. *J. R. Soc. Interface* **13**, 20160620 (2016).
11. M. Jadidi *et al.*, Mechanical and structural changes in human thoracic aortas with age. *Acta Biomater.* **103**, 172–188 (2020).
12. R. G. Koch *et al.*, A custom image-based analysis tool for quantifying elastin and collagen micro-architecture in the wall of the human aorta from multi-photon microscopy. *J. Biomech.* **47**, 935–943 (2014).
13. T. C. Gasser, R. W. Ogden, G. A. Holzapfel, Hyperelastic modelling of arterial layers with distributed collagen fibre orientations. *J. R. Soc. Interface* **3**, 15–35 (2006).
14. S. Baek, R. L. Gleason, K. R. Rajagopal, J. D. Humphrey, Theory of small on large: Potential utility in computations of fluid–solid interactions in arteries. *Comput. Methods Appl. Mech. Eng.* **196**, 3070–3078 (2007).
15. G. A. Holzapfel, J. A. Niestrawska, R. W. Ogden, A. J. Reinisch, A. J. Schriefl, Modelling non-symmetric collagen fibre dispersion in arterial walls. *J. R. Soc. Interface* **12**, 20150188 (2015).
16. D. Valdez-Jasso *et al.*, Analysis of viscoelastic wall properties in ovine arteries. *IEEE Trans. Biomed. Eng.* **56**, 210–219 (2009).
17. G. Franchini, I. D. Breslavsky, G. A. Holzapfel, M. Amabili, Viscoelastic characterization of human descending thoracic aortas under cyclic load. *Acta Biomater.* **130**, 291–307 (2021).
18. G. A. Holzapfel, T. C. Gasser, M. Stadler, A structural model for the viscoelastic behavior of arterial walls: Continuum formulation and finite element analysis. *Eur. J. Mech. A, Solids* **21**, 441–463 (2002).
19. M. Amabili, P. Balasubramanian, I. Breslavsky, Anisotropic fractional viscoelastic constitutive models for human descending thoracic aortas. *J. Mech. Behav. Biomed. Mater.* **99**, 186–197 (2019).
20. M. E. Safar, Arterial stiffness as a risk factor for clinical hypertension. *Nat. Rev. Cardiol.* **15**, 97–105 (2018).
21. A. J. Bank *et al.*, Contribution of collagen, elastin, and smooth muscle to in vivo human brachial artery wall stress and elastic modulus. *Circulation* **94**, 3263–3270 (1996).
22. A. H. Betrie *et al.*, Zinc drives vasorelaxation by acting in sensory nerves, endothelium and smooth muscle. *Nat. Commun.* **12**, 3296 (2021).
23. P. H. Ratz, K. M. Berg, N. H. Urban, A. S. Miner, Regulation of smooth muscle calcium sensitivity: KCl as a calcium-sensitizing stimulus. *Am. J. Physiol. Cell Physiol.* **288**, C769–C783 (2005).
24. R. L. Armentano, J. G. Barra, J. Levenson, A. Simon, R. H. Pichel, Arterial wall mechanics in conscious dogs. Assessment of viscous, inertial, and elastic moduli to characterize aortic wall behavior. *Circ. Res.* **76**, 468–478 (1995).
25. P. B. Dobrin, A. A. Rovick, Influence of vascular smooth muscle on contractile mechanics and elasticity of arteries. *Am. J. Physiol.* **217**, 1644–1651 (1969).
26. P. B. Dobrin, Mechanical behavior of vascular smooth muscle in cylindrical segments of arteries in vitro. *Ann. Biomed. Eng.* **12**, 497–510 (1984).
27. R. H. Cox, Effects of norepinephrine on mechanics of arteries in vitro. *Am. J. Physiol.* **231**, 420–425 (1976).
28. M. A. Gaballa *et al.*, Large artery remodeling during aging: Biaxial passive and active stiffness. *Hypertension* **32**, 437–443 (1998).
29. P. Fridez *et al.*, Adaptation of conduit artery vascular smooth muscle tone to induced hypertension. *Ann. Biomed. Eng.* **30**, 905–916 (2002).
30. F. M. L. Attinger, Two-dimensional in-vitro studies of femoral arterial walls of the dog. *Circ. Res.* **22**, 829–840 (1968).
31. J. T. Herlihy, R. A. Murphy, Length-tension relationship of smooth muscle of the hog carotid artery. *Circ. Res.* **33**, 275–283 (1973).
32. S. Yang, Q. Wu, S. Huang, Z. Wang, F. Qi, Sevoflurane and isoflurane inhibit KCl-induced class II phosphoinositide 3-kinase α subunit mediated vasoconstriction in rat aorta. *BMC Anesthesiol.* **16**, 63 (2016).
33. A. Rachev, K. Hayashi, Theoretical study of the effects of vascular smooth muscle contraction on strain and stress distributions in arteries. *Ann. Biomed. Eng.* **27**, 459–468 (1999).
34. M. A. Zulliger, A. Rachev, N. Stergiopulos, A constitutive formulation of arterial mechanics including vascular smooth muscle tone. *Am. J. Physiol. Heart Circ. Physiol.* **287**, H1335–H1343 (2004).
35. H. P. Wagner, J. D. Humphrey, Differential passive and active biaxial mechanical behaviors of muscular and elastic arteries: Basilar versus common carotid. *J. Biomech. Eng.* **133**, 051009 (2011).
36. S. C. Murtada, A. Arner, G. A. Holzapfel, Experiments and mechanochemical modeling of smooth muscle contraction: Significance of filament overlap. *J. Theor. Biol.* **297**, 176–186 (2012).
37. S.-I. Murtada, S. Lewin, A. Arner, J. D. Humphrey, Adaptation of active tone in the mouse descending thoracic aorta under acute changes in loading. *Biomech. Model. Mechanobiol.* **15**, 579–592 (2016).
38. D. C. Haspinger, S.-I. Murtada, J. A. Niestrawska, G. A. Holzapfel, Numerical analyses of the interrelation between extracellular smooth muscle orientation and intracellular filament overlap in the human abdominal aorta. *Z. Angew. Math. Mech.* **98**, 2198–2221 (2018).
39. J.-L. Gade, C.-J. Thore, B. Sonesson, J. Stålhand, In vivo parameter identification method for arteries is extended to account for smooth muscle activity. *Biomech. Model. Mechanobiol.* **20**, 1547–1559 (2021).
40. G. A. Holzapfel, T. C. Gasser, R. W. Ogden, A new constitutive framework for arterial wall mechanics and a comparative study of material models. *J. Elast.* **61**, 1–48 (2000).
41. I. Breslavsky, G. Franchini, M. Amabili, Effect of fiber exclusion in uniaxial tensile tests of soft biological tissues. *J. Mech. Behav. Biomed. Mater.* **112**, 104079 (2020).
42. P. Lacolley, V. Regnault, P. Segers, S. Laurent, Vascular smooth muscle cells and arterial stiffening: Relevance in development, aging, and disease. *Physiol. Rev.* **97**, 1555–1617 (2017).
43. S. K. Michael *et al.*, High blood pressure arising from a defect in vascular function. *Proc. Natl. Acad. Sci. U.S.A.* **105**, 6702–6707 (2008).
44. F. V. Brozovich *et al.*, Mechanisms of vascular smooth muscle contraction and the basis for pharmacologic treatment of smooth muscle disorders. *Pharmacol. Rev.* **68**, 476–532 (2016).